Saturation effect in the excitation of heliumlike Si projectiles in the intermediate velocity range

U. Tiwari,[1] A. K. Saha,[1] L. C. Tribedi,[1] M. B. Kurup,[1] P. N. Tandon,[1] and L. Gulyas[2]
[1]*Tata Institute of Fundamental Research, Homi Bhabha Road, Mumbai 400 005, India*
[2]*Institute of Nuclear Research of the Hungarian Academy of Sciences (ATOMKI), P.O. Box 51, H-4001 Debrecen, Hungary*
(Received 29 June 1998)

The saturation effect in the excitation cross sections has been investigated for Si^{12+} ions colliding with gas target atoms (atomic number Z_t between 2 and 54) in the (8–12)-a.u. velocity range, both experimentally and theoretically. The experimental excitation cross sections have been deduced from the measured Ly x rays following the decay of the excited atoms. Theoretical calculations have been performed using the first Born approximation, the symmetric eikonal continuum distorted wave (SECDW) approximation, and the Schwinger variational principle (SVP). Similar to the earlier observations on the heavier ion species, the saturation has been found in both the experimental and the SVP cross sections in the entire velocity range. The SECDW approximation, however, has been found to underestimate the cross sections at large values of Z_t in the presently investigated systems. In the light of these findings, the role of higher-order effects within different theoretical models has been reviewed and the possible interaction mechanisms have been discussed.
[S1050-2947(98)00112-7]

PACS number(s): 34.50.Fa, 34.10.+x, 34.90.+q

I. INTRODUCTION

Inner-shell processes in ion-atom collisions have been extensively studied in the past, both experimentally and theoretically, covering a wide range of impact velocities. In the low velocity range (defined by an impact velocity v much less than an active electron orbital velocity v_e) and the high velocity range ($v \gg v_e$), only one of the processes, the electron capture in the former and ionization/excitation in the latter, is dominant and these are reasonably well understood within the existing theoretical models [1,2]. In the intermediate velocity region ($v \sim v_e$), on the other hand, all these processes are of the same order and, in most cases, influence each other quite strongly. Moreover, depending upon the strength of the perturbing field, these may also move from a perturbative regime to a strongly interacting regime. The theoretical interpretation of the experimental observations in terms of individual processes is thus rather difficult. To understand the interaction mechanism in this velocity region, numerous investigations have been made in the past, on electron capture as well as on ionization, on a variety of collision systems including light and heavy accelerated ion beams. In comparison, however, the studies related to the excitation of electrons to the bound states have mostly been confined only to the one- and two-electron (H and He) atoms [3,4]. In many-electron atoms, unlike ionization, the excitation channels are very much limited (the lowest outer shells are filled) and, moreover, difficult to separate from the ionization channel. With the use of high-energy accelerators, however, this difficulty has been overcome recently and experiments have also been extended to the excitation of partially stripped heliumlike (fully vacant outer shells) high-Z ions. In one of the early measurements, carried out by Brendlé and co-workers [5,6], the K-shell excitation of Fe^{24+} ions at an impact velocity of 17 a.u. was investigated in collision with He, N_2, Ar, and Kr gas targets. Later this group extended these investigations to 37-a.u. Kr^{34+} projectile ions [7]. Here an estimate of the multistep processes was also made and incorporated in order to derive the single-electron excitation cross sections. Very recently, an accurate measurement of the excitation cross sections on 23-a.u. Ar^{16+} ions has also been reported by Vernhet *et al.* [8,9], where the various single- and multistep processes contributing to the Ly spectrum have been separately identified using a high-resolution crystal spectrometer. A striking feature of all these measurements is the observed saturation in the excitation cross sections at high values of the perturbing target nuclear charge Z_t. A similar saturation is also seen in the measurements reported by Xu *et al.* [10] on 18.5-a.u. Ca^{18+} projectiles.

In contrast to the first Born approximation (FBA) predicted Z_t^2 dependence, the observed saturation in the excitation function was explained by Brendlé *et al.* [5], and by Gayet and Bouamond [11] using a theory based on the fractional form of the Schwinger variational principle [12]. A similar saturation was also shown later within the distorted wave approximation by Mukoyama and Lin [13]. The asymptotic convergence of the excitation cross sections obtained within different theoretical frameworks has conceptually been attributed to the incorporation of higher-order effects, unaccounted for in the first-order theories.

It should, however, be stressed here that the few experimental studies mentioned above have all been carried out at a single impact velocity for each projectile ion and there are no other experimental measurements, to our knowledge, to substantiate other various aspects, such as the impact velocity dependence, of these theoretical models related to the excitation process. Moreover, the measurements have so far been carried out only on systems with $Z_t/Z_p \leqslant 3$. It is thus desirable to have more measurements not only at different impact velocities but also on more projectile ion species (especially the lighter projectiles that would enhance the Z_t/Z_p ratio) in order to test the predictions of the different theoretical models.

In the present paper we report the measurements on the excitation of Si^{12+} ions in the (8–12.5)-a.u. velocity range, in collision with He, N_2, Ne, Ar, and Xe targets. In addition,

we also present the results obtained from three theoretical models, the first Born approximation, the symmetric eikonal continuum distorted wave (SECDW) approximation, and the Schwinger variational principle (SVP), and discuss them in the light of the present experimental observations.

In Sec. II the experimental setup is described and the method of evaluation of the excitation cross section from the observed Ly x-ray spectrum is discussed. The procedure for the application of two theoretical models, the SECDW approximation and the Schwinger variation principle, to the present system is discussed briefly in Sec. III. The experimental and theoretical results are presented in Sec. IV. On the basis of these findings, we discuss in Sec. V the possible interaction mechanisms. We conclude in Sec. VI.

II. EXPERIMENTAL AND ANALYTICAL PROCEDURE

A. Experimental setup

The details of the experimental setup used in these measurements have been described earlier by Saha *et al.* [14]. Briefly, the ion beams of Si in the energy range 45–110 MeV were obtained from the BARC-TIFR Pelletron accelerator at Mumbai. The beam was further stripped using a foil stripper placed before the switching magnet. The well collimated ion beam, ~ 2 mm in diameter, was made to interact at right angles with an effusive jet of the target gas emanating from a capillary at a vertical distance of 4 mm from the beam trajectory. The jet assembly, mounted on the top flange of a differentially pumped chamber, had the provision for movement in the X and Y directions to enable perfect alignment of the x-ray detectors with respect to the intersection region between the gas jet and the incoming beam. The gas pressure in the capillary was continuously monitored and controlled using a capacitance manometer and a solenoid valve. Some measurements were also done using a gas cell that replaced the jet assembly. The base pressure in the scattering chamber was kept $\sim 10^{-6}$ torr. The x rays were detected with two Si(Li) x-ray detectors (with a full width at half maximum of approximately 160 eV at 5.9 keV) placed at 90° with respect to the beam direction. The detectors were kept outside the scattering chamber at a distance of 2.5 cm from the interaction center. An extended collimator of 5 mm diameter and 8 mm length was placed in front of the x-ray detectors to define the interaction volume from where the x rays were recorded by the detector. In this geometry the detectors view a solid angle $\Omega/4\pi$ of 8×10^{-4} and a path length of 1 cm of the projectile beam. The x-ray spectra were always recorded with and without the target gas to correct for the projectile x-ray background originating from the residual gas pressure in the chamber. In order to obtain the absolute values of the cross sections, the target thickness overlapping with the projectile beam was determined by measuring the Ly x-ray production cross sections in Ar atoms with 36-MeV and 56-MeV F^{9+} ions in the same experimental geometry. The target thickness was obtained by comparing these with the reported cross sections for the same system by Hopkins *et al.* [15]. All measurements were carried out at several gas pressures, maintaining the single-collision condition.

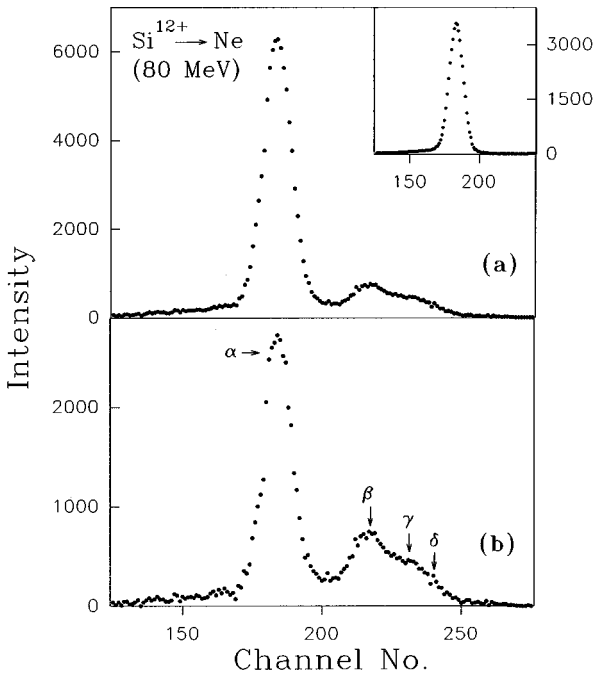

FIG. 1. (a) As-recorded Ly spectrum of 80-MeV Si^{12+} ions in the case of a Ne target. The corresponding background spectrum arising from the decay of the metastable ions is shown in the inset. (b) The spectrum after the background subtraction. Here the different Ly components are also indicated.

B. X-ray production cross sections

The x-ray production cross sections of the He-like Si^{12+} ions have been deduced from the recorded Ly spectra. A typical, as recorded, x-ray spectrum of 80-MeV Si^{12+} ions interacting with a Ne target is shown in Fig. 1(a). In the inset of this figure, we show the corresponding background spectrum recorded in the absence of the target gas. The background spectrum contains predominantly the Ly-α component and arises due to the spontaneous decay of the metastable ions present in the ion beam. The $2\,^1S_0$, $2\,^3S_1$, and $2\,^3P_{0,1,2}$ states are the known metastable states in the two-electron ions. In the present experiments these states are formed at the post-foil stripper where the beam of ions obtained from the pelletron accelerator is further stripped to get He-like ions. In Si^{12+}, all these states except $2\,^3S_1$ have a lifetime of at most a few nanoseconds and decay (either to the ground state or to the $2\,^3S_1$ state) much before the interaction region, situated ~ 15 m downstream from the foil stripper. However, the metastable $2\,^3S_1$ state has a lifetime of ~ 2.6 μs [16] and a fraction of ions formed in this state remain with the ion beam in the interaction region. The decay of these metastable ions in the region viewed by the detectors produces Ly-α x rays, indistinguishable from those produced by the ion-atom interaction. In the presence of these metastable ions, the total Ly x-ray production cross section σ_t^{Ly}, obtained after the subtraction of the background spectrum [Fig. 1(b)], can be decomposed as

$$\sigma_t^{Ly} = (1-x)\sigma^{Ly} + x\sigma_m^{Ly}, \tag{1}$$

where σ^{Ly} and σ_m^{Ly} are the Ly x-ray production cross sections interacting with the target atoms of He-like ions (both

the electrons in the K shell) and the two electron metastable ions (one electron in the K shell and the other in the $2\,^3S_1$ state), respectively, and x is the fraction of ions in the metastable state just before the scattering region.

Contribution from the metastable ions ($x\sigma_m^{Ly}$)

The excitation cross sections have been deduced from the x-ray production cross sections σ^{Ly} of the He-like ions in the ground state. To obtain σ^{Ly} from σ_t^{Ly}, x and σ_m^{Ly} were estimated separately. The fraction x was obtained from the recorded background spectrum and the known lifetime of the metastable state using the expression

$$x=\frac{4\pi\Delta N\tau_0 v}{Nl\Omega_x\epsilon_x}, \tag{2}$$

where ΔN is the number of Ly x-ray counts in the background spectrum (due to the decay of the metastable ions), N the total number of incident ions (determined from the charge collected in the Faraday cup), τ_0 the lifetime of the metastable state, v the velocity of the projectile ions, l the path length of the ion beam viewed by the x-ray detector, Ω_x the solid angle, and ϵ_x the efficiency of the x-ray detector. This fraction was also inferred independently from the enhancement in the Ar K x-ray yield in an interaction with the Si^{12+} ion beam. This enhancement is caused by the K-K transfer channel [17], which is open for the metastable ions having a vacancy in the K shell. Both ways the fraction x has been found to be $17(\pm 1)\%$.

The x-ray production cross sections of the metastable Si^{12+} ions σ_m^{Ly} was estimated from the measured x-ray production cross sections of Si^{13+} ions. The metastable Si^{12+} ions and Si^{13+} ions both have a vacancy in the K shell and except for the difference in their charge state, their Lyman spectra in an interaction with a target are exactly identical. Thus, to estimate σ_m^{Ly}, the corresponding x-ray production cross sections for Si^{13+} ions were also measured. These were then corrected using the empirically known $q^{3.9}$ dependence [18] to obtain σ_m^{Ly}.

The major contribution to the x-ray production in Si^{13+} ions comes from the direct capture, which is quite large in the velocity range examined in the present experiments. Thus the relative contribution of the metastable ions to the total Ly x-ray production is also large. In collision with Ar atoms, for example, it has been found to vary from $\sim 25\%$ to 65% in the energy range $110-45$ MeV, while with Xe as the target it varies from 32% to 78% in the same energy range.

C. Excitation cross sections

The method of evaluating the single-electron excitation cross section from the x-ray production cross section of He-like ions has been described by Chabot *et al.* [7]. There are various processes that contribute to the Lyman spectrum of the He-like ions in their interaction with the neutral target atoms. Restricting to one- and two-electron processes, these are single-electron excitation, double-electron excitation, ionization excitation, and capture ionization (CI). In capture ionization, one of the projectile electrons gets ionized, creating a vacancy in the K shell and simultaneously a target electron is captured in one of the higher states, which then decays to produce Ly x ray. Thus the total x-ray production cross section σ^{Ly} can be expressed in terms of the individual cross sections related to these processes as

$$\sigma^{Ly}=(1-\tau)(\sigma_{SE}+2\omega\sigma_{DE}+\sigma_{IE})+(1-\tau')\sigma_{CI}. \tag{3}$$

The quantities τ and τ' are the fractions of ions populated in the metastable states (in an interaction with the target) by direct excitation and capture ionization, respectively, which do not decay within the view of the x-ray detector, and ω is the fluorescence yield in doubly excited He-like ions. A factor of 2 appears with σ_{DE} because a doubly excited state produces two Ly x rays.

Within the independent-particle approximation, Eq. (3) can be simplified as [7]

$$\sigma^{Ly}=2(1-\tau)\sigma_E+(1-\tau')\sigma_{CI}, \tag{4}$$

where

$$\sigma_E=2\pi\int b\,db\,P_E(b) \tag{5}$$

is the excitation cross section in a one-electron ion. Here b is the impact parameter.

Contribution from capture ionization [$(1-\tau')\sigma_{CI}$]

The CI contribution to the total Ly x-ray production cross sections has been evaluated in an approximate manner from the measured capture cross sections and the estimated ionization cross sections and using the corresponding impact parameter dependent probabilities as

$$\sigma_{CI}=2\pi\int 2b\,db\,P_C(b)P_I(b). \tag{6}$$

The ionization and capture probabilities were assumed to have the analytical form $P(b)=P(0)e^{-b/a}$ [6], where a is the electron radius in its initial shell.

To obtain the capture probabilities, the capture cross sections were experimentally measured for Si^{13+} ions and the results extended to Si^{12+} ions assuming a $q^{3.9}$ dependence [18]. The ionization cross section with the He target was calculated using the perturbed-stationary-state theory with energy-loss, Coulomb deflection, and relativistic corrections (ECPSSR) [19], which is known to be correct for small perturbation [20]. The same model, however, could not be applied to high-Z targets where the first Born approximation is no longer valid. To estimate the ionization cross section with other targets we have made an assumption that the excitation cross section to high-n states and to the continuum (i.e., ionization) follow a similar Z_t dependence. Hence the ionization cross sections with all the other targets were obtained from the excitation cross sections in the $n=3$ state and scaling them using the ECPSSR ionization cross section for the helium target. The excitation cross sections in the $n=3$ state were calculated using the Schwinger variational principle, discussed later.

It should be noted that the capture-ionization cross section obtained this way includes the prefactor $1-\tau'$ appearing in Eq. (4). This is because the states formed by a direct capture

in Si^{13+} are identical to those formed by capture ionization in Si^{12+} with a similar nl state distribution and an equal metastable state fraction.

The estimated CI contribution to σ^{Ly} with Xe target is $\sim$30% for 80-MeV ions and becomes $\sim$50% for 45-MeV ions. The corresponding fractions for Ar are 13% and 20%, respectively.

D. Metastable and cascading corrections

After the subtraction of the CI contribution, the evaluation of the total excitation cross section σ_E from the Ly x-ray production cross section σ^{Ly} needs a correction for the undetected population in the metastable states. As the direct excitation populates only the singlet states, the only metastable state is $2\,^1S_0$. This state is populated not only by direct excitation but also by feeding from the higher ($n \geqslant 3$) states. The feeding correction has been taken into account by enhancing the intensity under β and the higher-order peaks in the Ly spectrum by a factor of $1/(1-f)$. The feeding fraction f has been estimated from the hydrogenic branching ratios tabulated by Omidvar [21] and is found to be 0.118 ± 0.002 for all the $np(n \geqslant 3)$ states. However, the fraction of metastable states excited directly during an interaction with the target could not be determined experimentally. So the total excitation cross sections presented in Sec. IV correspond to direct excitation in all states except in $2\,^1S_0$.

To determine the excitation cross sections to the individual np states, the intensities in the corresponding resolved Ly components need a correction both for the branching to the lower states (other than $1s$) and for the feeding from the higher states. The branching correction has been done using the known hydrogenic branching ratios [21]. However, except for the $n'p \rightarrow np(n' \geqslant n+2)$ states, the feeding contribution, which depends on the $n'l$ excited-state distribution, has not been estimated. In the absence of the feeding correction, the individual excitation cross sections $\sigma(1s \rightarrow 2p+)$ and $\sigma(1s \rightarrow 3p+)$ obtained from the resolved components of the Lyman spectrum, actually correspond to the composite states. The corresponding theoretical cross sections have been constructed from the $1s \rightarrow nl$ excitation cross sections $\sigma(nl)$ using the hydrogenic branching ratios as

$$\sigma(1s \rightarrow 2p+) = \sigma(2p) + \sigma(3s) + \sigma(3d) + 0.584\sigma(4s) + \cdots, \tag{7}$$

$$\sigma(1s \rightarrow 3p+) = \sigma(3p) + 0.416\sigma(4s) + \cdots. \tag{8}$$

III. THEORETICAL CALCULATIONS

Apart from the first Born approximation, the excitation cross sections have also been estimated using the SVP and the SECDW approximation. In the fractional form of the Schwinger variational principle [12] the scattering amplitude for the transition between the states $\alpha \rightarrow \beta$ is given as

$$A_{\beta\alpha}(b) = -\frac{i}{v}\frac{\langle \beta | V_T | \psi_\alpha^+ \rangle \langle \psi_\beta^- | V_T | \alpha \rangle}{\langle \psi_\beta^- | V_T - V_T G^+ V_T | \psi_\alpha^+ \rangle}, \tag{9}$$

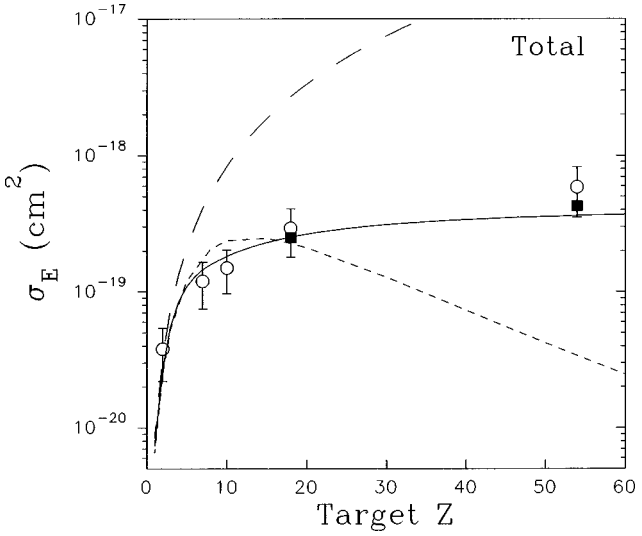

FIG. 2. Experimental and theoretical total excitation cross sections per electron into all the states except the $2s$ state of 80-MeV Si^{12+} projectiles as a function of the target atomic number: circle and filled squares are the experimental results without and with CI correction, respectively; the solid curve is the prediction of the Schwinger theory; long-dashed and short-dashed curves are the FBA and SECDW predictions, respectively. The error bars on the experimental data points include the statistical errors in determining the metastable fraction and in the fitting of the Ly spectra and also the uncertainty in the target thickness measurement ($\sim$25%).

where ψ_α^+ and ψ_β^- are the scattering wave functions defined by the eikonal Lippman-Schwinger equations and G^+ is the Green's function operator [12]. By expanding ψ_α^+ and ψ_β^- on the basis sets $\{|i\rangle\}$ and $\{|j\rangle\}$, respectively, of dimension N each, the transition amplitude can be expressed as [11]

$$A_{\beta\alpha}(b) = -\frac{i}{v}\sum_{i=1}^{N}\sum_{j=1}^{N}\langle \beta | V_T | i \rangle (D^{-1})_{ij} \langle j | V_T | \alpha \rangle, \tag{10}$$

where $(D^{-1})_{ij}$ is the element (i,j) of the matrix D^{-1}, the inverse of matrix D, defined by the elements

$$D_{ji} = \langle j | V_T - V_T G^+ V_T | i \rangle. \tag{11}$$

Using this formulation, the numerical and analytical procedure to calculate the excitation cross section in an ion-atom collision was developed by Brendlé *et al.* [5]. A similar numerical code following the procedure described in Ref. [11] has also been developed by us, which reproduces their results within 10%. In the evaluation of the Schwinger transition amplitude, mainly two kinds of matrix elements are to be calculated: the first Born-like elements $\langle j | V_T | i \rangle$ and the second Born-like elements $\langle j | V_T G_T^+ V_T | i \rangle$. In the present calculations we have used hydrogenic wave functions to evaluate these and coupled them in accordance with Eq. (10) to obtain the Schwinger transition amplitudes. The cross sections were then calculated by integrating over the impact parameter.

The results of these calculations are shown in Figs. 2 and 4 for the total excitation and in Figs. 3 and 5 for excitation to the $3p+$ states. For excitation in a given nl state, the basis sets $\{|i\rangle\}$ and $\{|j\rangle\}$ consisted of five elements: the ground

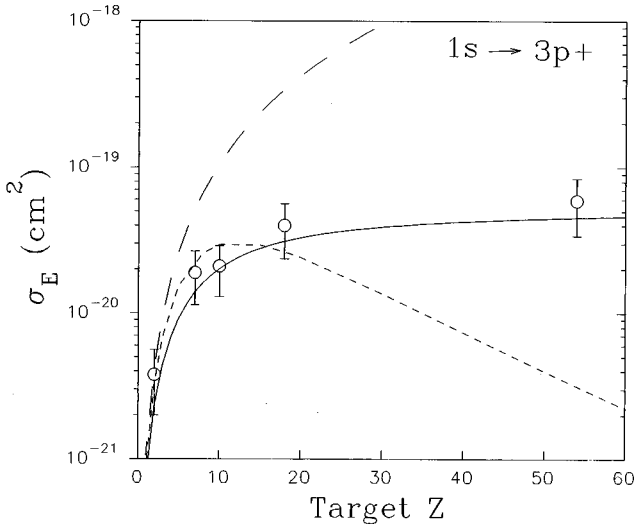

FIG. 3. Same as in Fig. 2 except for the $1s \rightarrow 3p+$ (see Sec. II D for the details) excitation.

state $1\,^1S_0$ and almost degenerate $n\,^1S_0$ and $n\,^1P_{1,0,-1}$ states. In the calculation of the second Born-like elements, all the states up to $n \leqslant 4$ were included as the intermediate states.

The continuum distorted wave (CDW) method has been applied in the symmetric eikonal configuration, as described in [22]. In the present calculations, the analytical potential from Green, Sellin, and Zachor [23] has been taken as the potential for the He-like ions and the excited-state wave functions have been obtained by solving numerically the time-independent Schrödinger equation. The targets have been treated as bare ions. The results of these calculations are shown in Figs. 2 and 4 for the total excitation cross sections and in Figs. 3 and 5 for the excitation to the $3p+$ state.

IV. RESULTS AND DISCUSSION

The total experimental excitation cross sections of 80-MeV Si^{12+} ions interacting with He, N_2, Ne, Ar, and Xe targets are shown in Fig. 2, with and without a CI correction. The corresponding values are also given in Table I. The CI-corrected data points are shown only for Ar and Xe targets where this contribution is significant. For other targets the CI correction is very small. The corresponding theoretical cross sections obtained from the first Born approximation, the SECDW approximation, and the Schwinger variational principle are also shown in Fig. 2. These were explicitly calculated for all the states up to $n \leqslant 3$. For other states, these were estimated using the $1/n^3$ dependence. Only with the He target do the experimental cross sections agree with the FBA results. In fact, in this limit of low perturbation strength the other theories also merge with the first Born approximation. However, as Z_t increases, the experimental cross sections deviate and remain much below the first Born quadratic function. The SECDW approximation correctly follows this deviation at least up to neon ($Z_t = 10$). However, as Z_t increases, the excitation function in this approximation starts decreasing again, with a maximum at $Z_t \sim 12$. This behavior is in contrast to the experimental observation where the cross sections tend to saturate to a finite value. This saturation in the excitation function is explained only within the SVP framework, where the agreement is good even at the larger values of Z_t.

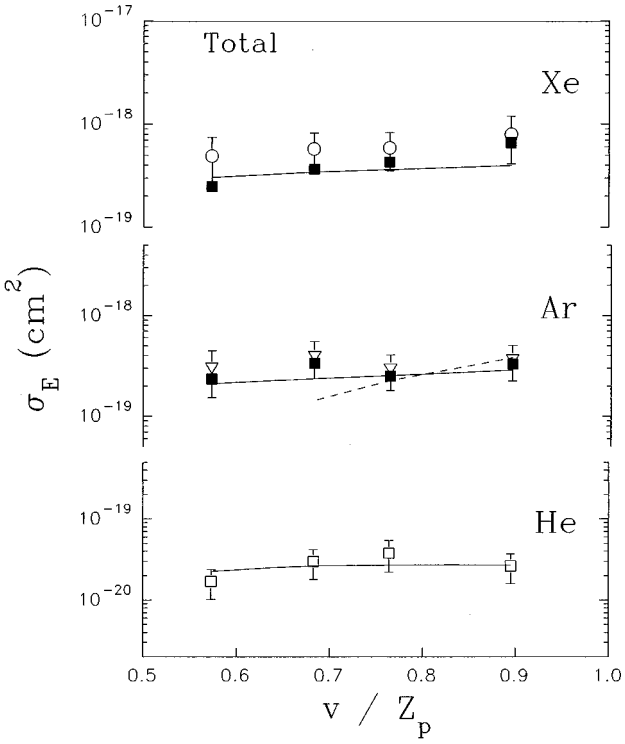

FIG. 4. Experimental and theoretical total excitation cross sections as a function of the reduced projectile velocity in the case of He, Ar, and Xe targets. The symbols have the same meaning as in Fig. 2.

A similar pattern in the experimental and the theoretical behavior has been found in the excitation to the individual

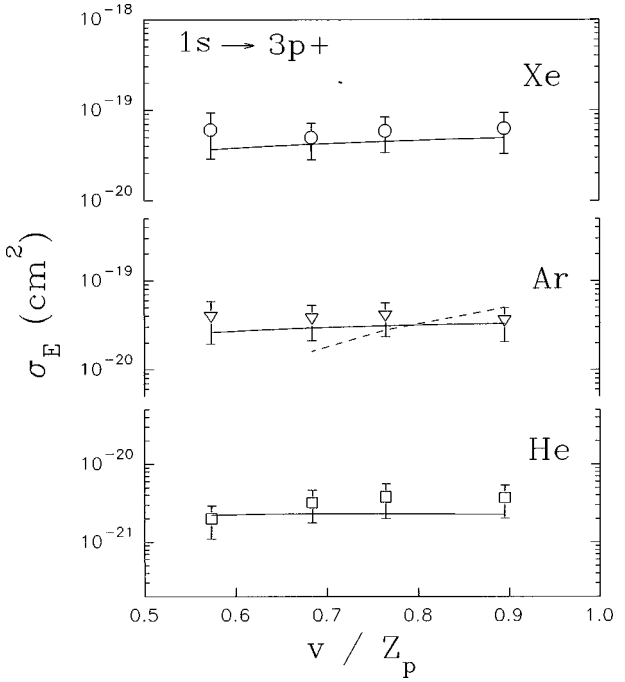

FIG. 5. Same as in Fig. 4 except for the $1s \rightarrow 3p+$ (see Sec. II D for the details) excitation.

TABLE I. Total excitation cross sections per electron for (45–110)-MeV Si^{12+} ions in an interaction with the gas targets, in units of 10^{-20} cm^2. The error bars on the data points are typically of the order of 40−50 %. The quantities in parentheses are the corresponding CI-corrected cross sections. The CI correction involving He, N, and Ne is very small.

Energy (MeV)	He	N	Ne	Ar	Xe
110	2.7		19	36 (32)	80 (66)
80	3.8	12	15	29 (25)	59 (43)
64	3.0	21	30	39 (34)	58 (37)
45	1.7			30 (23)	49 (25)

quantum states. The results for the excitation to the composite $3p+$ state (see Sec. II D for explanation) are shown in Fig. 3 and also in Table II. The theoretical cross sections were calculated using only the first two terms on the right-hand side of Eq. (8), which are most dominant. Again, only the SVP formulation agrees with the observed saturation behavior. The same is true for the other resolved Ly components.

The impact velocity dependence of the excitation function is another aspect that we have examined for the different values of Z_t, although in the present experimental conditions the ion energy could be varied only in the (45–110)-MeV range. The experimental cross sections for the Xe, Ar, and He targets are shown in Fig. 4 as a function of the reduced velocity v/Z_p. For the Xe target, the FBA and SECDW cross sections (not shown) lie much above and much below the corresponding experimental values, respectively. The SVP curve, on the other hand, agrees with the measured cross sections, particularly after the CI correction. For the Ar target ($Z_t=18$), both the SVP and the SECDW curves are shown in the figure. It can be seen that even in this case the SECDW underestimates the excitation cross sections at the lower velocities. In the case of the He target, on the other hand, all the theoretical curves have been found to match the experimental results and lie close to each other. For clarity, however, only the SVP curve is shown in the figure.

A similar behavior is found in the excitation to the $3p+$ states, as has been shown in Fig. 5. The agreement between the SVP predictions and the experimental cross sections in this case is, in general, better than that in the total cross sections.

The present results thus show that the saturation effect in the excitation cross sections continues even at much lower collision velocities and also in the lighter projectile ions. Moreover, the Schwinger variational principle reproduces it reasonably well in all the studied collision systems. This shows that the interaction mechanisms in all these systems are essentially the same. The relative importance of the different interaction mechanisms, however, may be dependent on the effective strength of the perturbation.

TABLE II. $1s\rightarrow 3p+$ excitation cross sections per electron for (45–110)-MeV Si^{12+} ions in an interaction with the gas targets, in units of 10^{-21} cm^2. The error bars on the data points are typically of the order of 45−55%.

Energy (MeV)	He	N	Ne	Ar	Xe
110	3.7		24	35	63
80	3.8	19	20	40	59
64	3.2	28	32	37	50
45	2.0			39	61

V. INTERACTION MECHANISMS

The saturation in the excitation cross sections, observed in the present systems at large values of Z_t, is similar to that reported by the Brendlé and co-workers for Kr^{34+}, Fe^{24+}, and Ar^{16+} ions. The agreement between the SVP predictions and the corresponding experimental results is also similar in the two cases. However, in terms of the theoretical description within the distorted wave formalism, our system is quite different from the previous ones. As has been shown by Mukoyama and Lin [13], the distorted wave approximation explains quite well the saturation in the excitation of the 400-MeV Fe^{24+} ions. In the 23-a.u. Ar^{16+} ions also, the SECDW approximation agrees with the experimental findings [9]. Similarly, we have found that the SECDW model developed by Gulyás and Fainstein [22] explains the saturation behavior in 34-MeV/nucleon Kr^{34+} ions also. However, in our systems, the same model predicts an entirely different behavior at large values of Z_t. We attribute this to the effective value of the perturbation strength S, which becomes quite large in our collision systems. We define S as

$$S=\frac{Z_t}{vZ_p}. \tag{12}$$

Physically, the perturbation strength is small at large collision velocity v and for the tightly bound electrons (i.e., for large Z_p). In our collision systems, the SECDW approximation remains valid up to $S\sim 0.1$, a value that has not been exceeded in the previous investigations to our knowledge. In the present cases the value of S becomes as large as 0.5. It is interesting to see, however, that the SVP formulation remains valid even at such large values of the perturbation strength.

In both the SVP and the CDW approximations, the first-order perturbation causes a linear enhancement in their transition amplitudes. The difference between the two, however, lies in their treatment of the additional perturbation effects. The CDW includes a Coulomb phase that decreases the transition amplitude by oscillating it along the ion trajectory. The frequency of oscillation is proportional to Z_t. Thus, as the strength of perturbation increases, there is a competition between the first-order enhancement in the transition amplitude and its decay due to the increased frequency of oscillation. At very small values of the perturbation strength, the former dominates and the cross sections increase quadratically with Z_t. At large perturbation strengths, on the other hand, the latter begins to dominate and the cross sections start decreasing. The maximum in the excitation function occurs when the effects of the two become equal.

In the SVP model, on the other hand, the higher-order perturbation effects are included explicitly in the form of a second Born-like term [see Eq. (9)]. This term in some way

introduces a coupling between the different states of the system, similar to the coupled-channel methods where the coupling is incorporated explicitly. In fact, the phenomenon of saturation has also been explained within the coupled-channel framework by Chabot *et al.* [7]. Here also the first-order perturbation increases the transition amplitudes linearly with Z_t. However, the coupling between the different states also increases with increasing Z_t. Thus a part of the excitation to a given state dissipates into all other states of the system, the dissipation being larger for higher values of Z_t. This interplay between the first-order enhancement in the transition amplitude and its dissipation into the system through the coupling among various channels produces the reported saturation in the coupled-channel description. In the fractional form of the SVP, such a dissipation is caused by the second Born-like term, which also decreases the transition amplitude. At large values of Z_t, the effect of this term completely neutralizes the enhancement caused by the first-order perturbation, resulting in a saturation in the excitation function. The saturation in the excitation function has been interpreted by Chabot *et al.* [7] in terms of an outward probability flow, i.e., the ionization of the electron through successive excitations. If this is true, then the ionization cross sections should show a corresponding enhancement at larger values of Z_t. This is, however, in contradiction to the experimental observations reported by Xu *et al.* [10] and Sant'Anna *et al.* [24] where the ionization cross sections also show a similar saturation. Thus we argue that the saturation is rather caused by the dissipation within the system through the coupling between the various channels.

VI. CONCLUSION

In conclusion, the excitation cross sections for (45–110)-MeV Si^{13+} ions have been measured in an interaction with the gas targets, with $2 \leqslant Z_t \leqslant 54$. In addition, the theoretical calculations have been carried out using the first Born approximation, the symmetric eikonal CDW approximation, and the Schwinger variational principle. In agreement with the SVP predictions, the saturation has been found in the experimental cross sections in the entire investigated velocity range. However, unlike in the previously investigated systems, the distorted wave formalism has been found to underestimate the cross sections at large values of Z_t. This has been attributed to the much larger values of the effective perturbation strength, realized only in the presently investigated systems. The saturation in the excitation function has been explained in terms of a dissipative mechanism arising due to the coupling among the various channels.

ACKNOWLEDGMENTS

We are thankful to S. Bandyopadhyay for his help in the initial part of the work. We also thank K. V. Thulasiram for his help during the measurements and the machine staff for smooth operation of the accelerator.

[1] M. Kimura and N. F. Lane, in *Advances in Atomic and Molecular Physics*, edited by D. Bates and B. Bederson (Academic, New York, 1989), Vol. 26, p. 79.
[2] J. S. Briggs and J. H. Macek, in *Advances in Atomic and Molecular Physics*, edited by D. Bates and B. Bederson (Academic, New York, 1990), Vol. 28, p. 1.
[3] W. Fritsch and P.D. Lin, Phys. Rep. **202**, 1 (1991).
[4] D. Detleffsen, M. Anton, A. Werner, and K. H. Schartner, J. Phys. B **27**, 4195 (1994); K. Reynmann, K. H. Schartner, B. Sommer, and E. Träbert, Phys. Rev. A **38**, 2290 (1988).
[5] B. Brendlé, R. Gayet, J. P. Rozet, and K. Wohrer, Phys. Lett. **54A**, 2007 (1985).
[6] K. Wohrer, A. Chetioui, J. P. Rozet, A. Jolly, F. Fernandez, C. Stephan, B. Brendlé, and R. Gayet, J. Phys. B **19**, 1997 (1986).
[7] M. Chabot, K. Wohrer, A. Chetioui, J. P. Rozet, A. Touati, D. Vernhet, M. F. Politis, C. Stephan, J. P. Grandin, A. Macias, F. Martin, A. Riera, J. L. Sanz, and R. Gayet, J. Phys. B **27**, 111 (1994).
[8] D. Vernhet, L. Adoui, J. P. Rozet, K. Wohrer, A. Chetioui, A. Cassimi, J. P. Grandin, J. M. Ramillon, M. Cornille, and C. Stéphan, Phys. Rev. Lett. **79**, 3625 (1997).
[9] D. Vernhet, J. P. Rozet, K. Wohrer, L. Adoui, C. Stéphan, A. Cassimi, and J. M. Ramillon, Nucl. Instrum. Methods Phys. Res. B **107**, 71 (1996).
[10] X. Y. Xu, E. C. Montenegro, R. Anholt, K. Danzmann, W. E. Meyerhof, A. S. Schlachter, B. S. Rude, and R. J. McDonald, Phys. Rev. A **38**, 1848 (1987).
[11] R. Gayet and M. Bouamoud, Nucl. Instrum. Methods Phys. Res. B **42**, 515 (1989).
[12] R. G. Newton, *Scattering Theory of Waves and Particles* (McGraw-Hill, New York, 1966), p. 317.
[13] T. Mukoyama and C. D. Lin, Phys. Lett. A **141**, 138 (1989).
[14] A. K. Saha *et al.*, J. Phys. B **31**, 1771 (1998).
[15] F. Hopkins, R. Brenn, A. R. Whittemore, N. Cue, V. Dutkiewicz, and R. P. Chaturvedi, Phys. Rev. A **13**, 74 (1976).
[16] R. Marrus and P. J. Mohr, Adv. At. Mol. Phys. **14**, 181 (1978).
[17] L. C. Tribedi, K. G. Prasad, P. N. Tandon, Z. Chen, and C. D. Lin, Phys. Rev. A **49**, 1015 (1994).
[18] A. S. Schlachter, J. W. Stearns, W. G. Graham, K. H. Berkner, R. V. Pyle, and J. A. Tanis, Phys. Rev. A **27**, 3372 (1983).
[19] W. Brandt and G. Lapicki, Phys. Rev. A **20**, 465 (1979); **23**, 1717 (1981), and references therein.
[20] H. Paul and J. Muhr, Phys. Rep. **135**, 47 (1986); G. Lapicki, J. Phys. Chem. Ref. Data **18**, 111 (1989).
[21] K. Omidvar, At. Data Nucl. Data Tables **28**, 1 (1983).
[22] L. Gulyás and P. D. Fainstein, Phys. Rev. A **56**, 1321 (1997).
[23] A. E. S. Green, D. L. Sellin, and A. S. Zachor, Phys. Rev. **184**, 1 (1969).
[24] M. M. Sant'Anna, W. S. Melo, A. C. F. Santos, G. M. Sigaud, and E. C. Montenegro, Nucl. Instrum. Methods Phys. Res. B **99**, 46 (1995).